Article

A Novel Method for Notable Reducing Phase Transition Temperature of VO$_2$ Films for Smart Energy Efficient Windows

Huan Guan, Dongping Zhang *, Yu Yang, Yi Liu, Aihua Zhong, Qicong He, Jiahua Qi and Ping Fan

Shenzhen Key Laboratory of Advanced Thin Films and Applications, College of Physics and Optoelectronic Engineering, Shenzhen University, Shenzhen 518060, China; guanhuan026@163.com (H.G.); yangyu2016@email.szu.edu.cn (Y.Y.); liuy@szu.edu.cn (Y.L.); zhongah@szu.edu.cn (A.Z.); 1800211011@email.szu.edu.cn (Q.H.); qijiahua883@163.com (J.Q.); fanping@szu.edu.cn (P.F.)
* Correspondence: zdpsiom@szu.edu.cn

check for updates

Abstract: Although Vanadium dioxide (VO$_2$) has a potential application value for smart energy efficient windows because of its unique phase transition characteristic, there are still many obstacles that need to be overcome. One challenge is to reduce its high transition temperature ($\zeta_c = 68\,°C$) to near room temperature without causing its phase transition performance degradation. In this paper, a novel method was employed that covered a 3 nm ultra-thin heavy Cr-doped VO$_2$ layer on the pure VO$_2$ films. Compared with the as-grown pure VO$_2$, obviously, phase transition temperature decreasing from 59.5 °C to 48.0 °C was observed. Different from previous doping techniques, almost no phase transition performance weakening occurred. Based on the microstructure and electrical parameters measurement results, the mechanism of ζ_c reducing was discussed. The upper ultra-thin heavy Cr-doped layer may act as the induced role of phase transition. With temperature increasing, carrier concentration increased from the upper heavy Cr-doped layer to the bottom pure VO$_2$ layer by diffusion, and induced the carrier concentration reach to phase transition critical value from top to bottom gradually. The present method is not only a simpler technique, but also avoids expensive alloy targets.

Keywords: vanadium dioxide; phase transition temperature; ultra-thin heavy Cr-doped layer

1. Introduction

Vanadium dioxide (VO$_2$) is one of the most interesting smart materials for its reversible metal-insulator transition (MIT) near room temperature ($\zeta_c = 68\,°C$) [1], in which optical, electrical, and other physical properties (transmittance, reflectance, emittance, refractive index, electrical resistivity etc.) [2,3] will be sharp changed by external stimuli (applied field or voltage [4], incident light [5], temperature variation [6], mechanical stress [7], pressure [8], etc.) in the transition process. These unique properties make VO$_2$ a suitable candidate for various technological potential applications in many fields, such as tunable filters [9], switching devices [10], memory materials [11], laser protection [12], ultrafast sensors [13], and Mott transistors [14]. Great attention has been attracted recently for the material both in scientific and technological applications.

In the last years, an increasing number of researches have been published and discussed VO$_2$-based applications. Among all the VO$_2$ application researches, the most attractive one is the smart energy efficient window application. Due to it exhibiting a reversible transformation from an infrared (IR)-transparent at low temperature semiconductor phase to an IR-reflective at high temperature

metallic phase, meanwhile maintaining visible transmittance, VO_2 is the most promising material for smart energy efficient windows [15]. Although lots of works have been done over the past years, still many obstacles should be overcome for VO_2-based smart window real applications. One challenge is to reduce the transition temperature ζ_c of VO_2 from 68 °C to around room temperature [16]. Previous reports showed that the ζ_c of VO_2 could be reduced by a range of technologies, such as elemental doping [17], introducing stress [18] and defects [19], and chemical stoichiometry adjustment [20]. Doping is considered to the most effective strategy to reduce the ζ_c of VO_2, especially for high-valence ions doping (such as Nb^{5+}, Mo^{6+}, W^{6+}, Tb^{3+}, etc.) [21–24]. Chae et al. [25] reported that the doped VO_2 with W and Ti using the sol-gel method led to a change of transition temperature and reduces the properties of MIT. M. Panagopoulou et al. [26] found that Mg doping could reduce the transition temperature of VO_2, and the 6 °C/at % Mg-doped VO_2 thin film on ZnO substrate presented the lower ζ_c around 35 °C, but the energy modulation had sharply decreased. Jin et al. [27] reported that doping W into VO_2 by using high-energy ion implantation appeared to have a much higher ζ_c reduction efficiency compared with other methods. Carlos Batista et al. [28] reported that the ζ_c would decrease 8 °C/at % by Nb doping. Most of previous works' results exhibited that the phase transition performance as well as solar energy modulation capability of VO_2 films weakened after doping, though the sharp decreasing of ζ_c was obtained.

In this work, pure VO_2 films were prepared by reactive pulsed magnetron sputtering, and a 3 nm ultra-thin heavy Cr-doped VO_2 layer was employed to cover on the prepared pure VO_2 film surface. By annealing in high vacuum environment at a temperature of 250 °C, notable phase transition temperature ζ_c reduction of VO_2 films was observed, while phase transition performance of the samples has hardly weakened. The present method is not only a simpler technique, but also avoidsexpensive alloy targets.

2. Experimental Details

VO_2 thin films were prepared on K_9 glass substrates at 440 °C by reactive pulsed direct current magnetron sputtering in vacuum chamber with turbo molecular bump system. High purity (99.99%) vanadium was used as target with diameter of 100 mm. First, the vacuum chamber was evacuated to a base pressure of 1.0×10^{-3} Pa before deposition. Then Ar (99.99%) and O_2 (99.99%) gases were led into chamber with flow rate of 40 sccm and 1.5 sccm acted as working gas and reactive gas, respectively. Before films' deposition, 10 minutes pre-sputtering was performed in Ar atmosphere to remove surface contaminant and oxide layer on the target in order to maintain deposition process stability and obtain high purity VO_2 films. A pulsed direct current supply (Advanced Energy Industries) was used for films magnetron sputtering deposition. The 50 nm thick VO_2 thin films were prepared under working pressure of 0.6 Pa. A 3 nm ultra-thin heavy Cr-doped VO_2 layer was deposited on the top of pure VO_2 films by direct current reactive co-sputtering method at room temperature with power of 10 W, and films' thickness was controlled by deposition time. Subsequently, the samples were annealed in high vacuum atmosphere (4.0×10^{-4} Pa) at 250 °C for 30 min. The schematic of thin films' preparation process is shown in Figure 1, and the samples are labeled as A, B, and C, respectively.
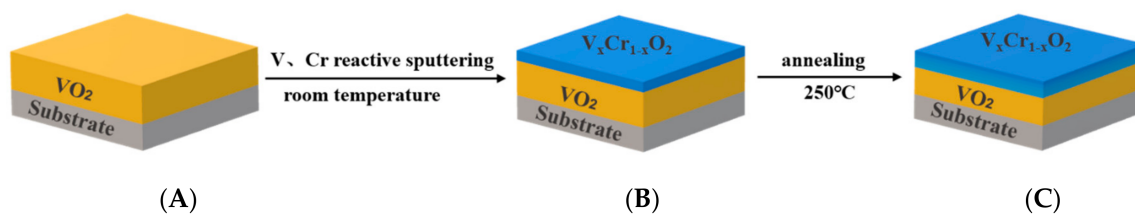

Figure 1. Schematic of the films structure, (**A**) is the pure VO_2 thin film, (**B**) is the unannealed Cr-doped VO_2 thin film, (**C**) is the Cr-doped VO_2 thin films annealing at 250 °C.

The transmittance thermal-hysteresis curves at $\lambda = 1550$ nm of the prepared samples were measured with a thin film phase transition measurement system (PERFECT PTM-1700, Perfect Opto-electronics Technology, Shenzhen, China), and the temperature ranged from room temperature to 90 °C. Microstructure of the films was identified by X-ray diffraction (XRD) in θ–2θ coupled scanning mode (Ultima IV, Rigaku, Tokyo, Japan) with Cu K$_\alpha$ radiation, which the wavelength is 0.15406 nm. The diffraction angle ranged from 10° to 80° with step by 0.02°. The vibrational modes in VO$_2$ films were examined by using Raman Microscopy (inVia, Renishaw, Gloucestershire, England) with a 532 nm wavelength laser as excitation source, and the laser power was kept as low as 2 mW in order to minimize additional heating effects, and the wave number range varied from 100 to 800 cm^{-1}. The transmittance of the thin films at room temperature and 80 °C were obtained using a spectrophotometer (UV-3600 PLUS, SHIMADZU, Shimadzu, Japan) in the range of 300–2500 nm. The samples surface morphologies were determined by field emission scanning electron microscopy (SEM). The temperature-dependent sheet-resistance variation of films was characterized using a four-point probe system, and the thin film temperature was ramped up from room temperature to 90 °C at a step of 1 °C in measurement process. The carrier concentration of the samples was measured by using the Hall Effect Measurement System (Bio Rad, HL5500 PC, Nanometrics, Milpitas, California, USA), and the entire sample was heated from 35 °C to 80 °C.

3. Result and Discussion

The thermochromism characteristics of VO$_2$ films were investigated by measuring their temperature dependence of IR transmittance at $\lambda = 1550$ nm. The transmittance-temperature dependence curves in the heating and cooling processes are shown in Figure 2a, and the transition temperature in the heating process ζ_{ch} and cooling process ζ_{cl} are shown in Figure 2b. The thermal hysteresis loop curves clearly exhibit that all samples have high phase transition performance. The transmittance at $\lambda = 1550$ nm changed from 65% in low temperature semiconductor state to 30% in high temperature metallic state. For sample A of the as-grown pure VO$_2$, the heating and cooling phase transition temperatures are $\zeta_{ch} = 67$ °C and $\zeta_{cl} = 52$ °C, respectively. The average phase transition temperature $\zeta_c = (\zeta_{ch} + \zeta_{cl})/2$ of sample A is 59.5 °C. When the sample surface was covered with an ultra-thin heavy Cr-doped layer, notable reducing of phase transition temperature was found, either unannealed or annealed. For the unannealed sample B, the ζ_c decreasing may be related to the interface stresses between the two layers. While for sample C, phase transition temperature further decreased from 54.5 °C to 48.0 °C after annealing. Figure 2a also shows that the phase transition amplitude almost keeps constant among the different samples.
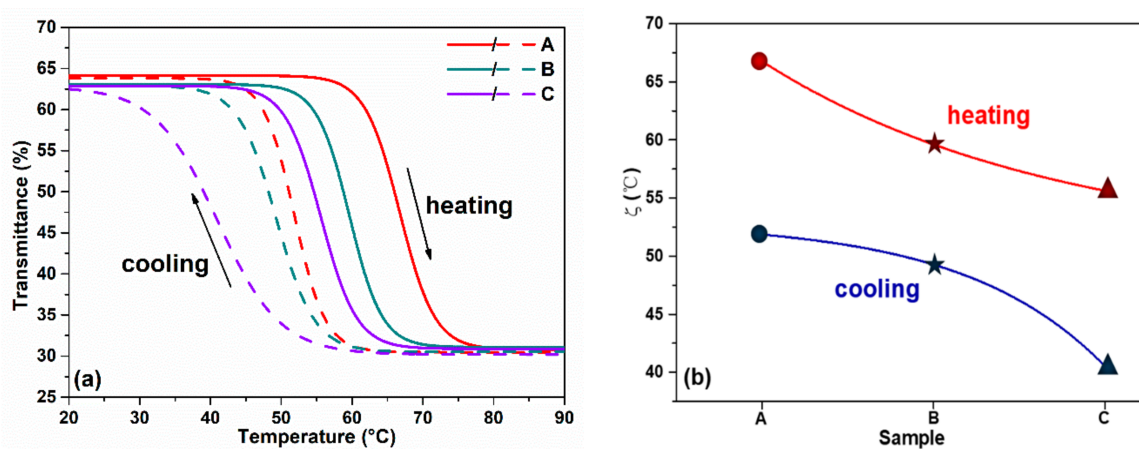

Figure 2. (**a**) Transmittance thermal hysteresis loop of all samples at $\lambda = 1550$ nm, (**b**) the ζ_{ch} and ζ_{cl} of all samples.

Figure 3 shows the transmittance spectra ranged from near ultraviolet to near-infrared region of the samples at ambient temperature and 80 °C, respectively. All the films show transmittance changes in the IR region after MIT. We also noticed that the transmittance spectra of the three samples are almost overlapped. Only a weak change of transmittance spectra was observed after being covered ultra-thin heavy Cr-doped layer. Combining the results of the above transmittance thermal hysteresis loop, we can conclude that the overlayer has not induced weakening of the phase transition performance. Based on the transmittance spectra, solar energy modulation ability of the samples was calculated according to the formula below [29]:

$$T_i = \frac{\int \phi_i(\lambda) T(\lambda) d\lambda}{\int \phi_i(\lambda) d\lambda} \tag{1}$$

$$\Delta T_{IR,sol} = T_{IR,sol}(20\ ^\circ C) - T_{IR,sol}(80\ ^\circ C). \tag{2}$$

where $T(\lambda)$ is the transmittance at wavelength λ, i denotes lum or sol, $\phi_{sol}(\lambda)$ is the solar irradiance spectrum at air mass 1.5, which likes the angle of incidence of sunlight is 37°, and $\phi_{lum}(\lambda)$ is the standard luminous efficiency function for the photopic vision of human eyes (380–780 nm). T_{sol} is effective utilization of solar energy in thin films, and $\Delta T_{IR,sol}$ is the solar energy modulation of VO$_2$ films in IR region, the region of 760–2500 nm is always chosen for calculation. According to the above formulas, the three samples have almost the same solar energy modulation capability of $\Delta T_{IR,sol} = 12\%$, which meets the requirement of the smart windows application.
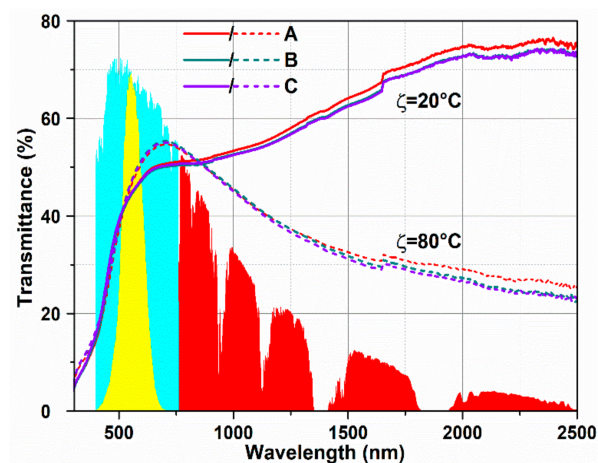

Figure 3. Optical transmittance spectra (300–2500 nm) at room temperature and 80 °C of the samples. The colored areas indicate the normalized values of spectral irradiance corresponding to the visible (blue) and near infrared radiation (red) ranges of solar spectra, and the yellow area indicates the values of eye sensitivity function.

Figure 4 shows the XRD spectra of the three different samples prepared with different procedures. The standard pattern of monoclinic (M) VO$_2$ (PDF#09-0142) is also present together for reference. In the XRD patterns, the peaks located at about $2\theta = 27.76°$ are corresponding to the characteristic pattern of VO$_2$, which shows the structure of monoclinic type with a (011) preferred orientation. The characteristic peaks of chromium oxides are not observed in sample B and C, indicating that chromium oxides in covered layer is too thin to detect, or Cr atoms entered the crystal lattice of VO$_2$ rather than a separate phase. We notice that the (011) diffraction peak position of 27.76° in our study lower than 27.86° of VO$_2$ powder from standard powder diffraction file (PDF) card, the residual stress may play the key role to the diffraction peak blue shifting.
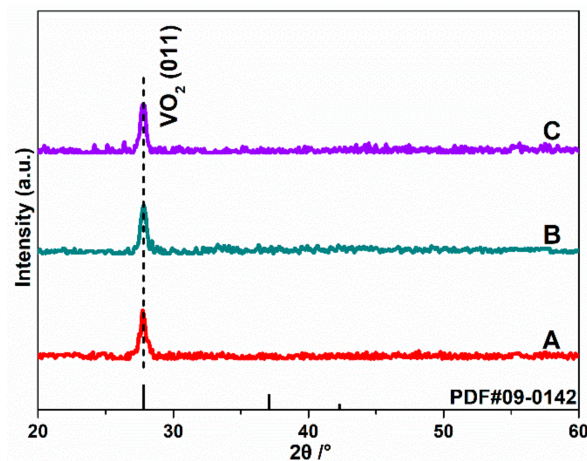
Figure 4. XRD patterns of all samples. (A) is the pure VO$_2$ thin film, (B) is the unannealed Cr-doped VO$_2$ thin film, (C) is the Cr-doped VO$_2$ thin films annealing at 250 °C.

Raman spectra of the VO$_2$ films at room temperature is shown in Figure 5. The spectra reveal that all samples have the same characteristic peaks, which appear at 193 cm^{-1}, 224 cm^{-1}, 308 cm^{-1}, 390 cm^{-1}, 498 cm^{-1}, and 614 cm^{-1}, identified to the VO$_2$ monoclinic phase [30]. No characteristic peaks of chromium oxides or other vanadium oxides appear, indicating that the main ingredient of films is VO$_2$, which can explain the temperature-transmittance hysteresis loop. The monoclinic phase is thus characterized by 18 Raman active modes with 9A$_g$ and 9B$_g$ modes [31]. Among 193 cm^{-1}, 224 cm^{-1}, 308 cm^{-1}, 498 cm^{-1}, and 614 cm^{-1} confirm the A$_g$ symmetry mode, another 390 cm^{-1} corresponds to the B$_g$ phonon mode [32]. This result is consistent with previous reports. The peaks at 193 cm^{-1}, 224 cm^{-1} are assigned to V-V vibration modes, whereas those in the high frequency of 308 cm^{-1}, 498 cm^{-1}, and 614 cm^{-1} are assigned to V-O vibration modes [33].
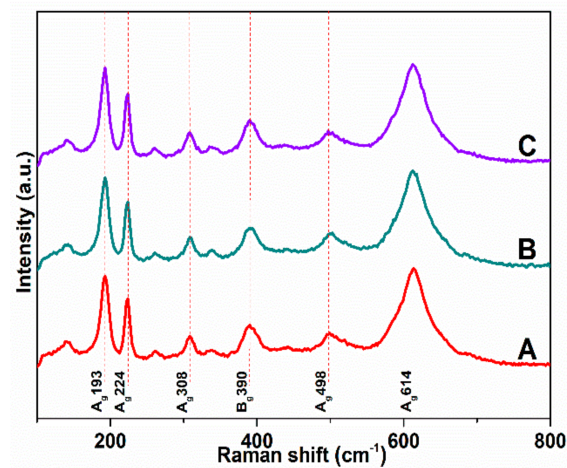

Figure 5. Raman spectra of all samples. (A) is the pure VO$_2$ thin film, (B) is the unannealed Cr-doped VO$_2$ thin film, (C) is the Cr-doped VO$_2$ thin films annealing at 250 °C.

Figure 6 shows the surface morphologies of the VO$_2$ film samples. All samples exhibit high crystallinity, continuous and dense structure, which are consistent with XRD results. For as-grown pure VO$_2$ sample A, some nanorods discontinuous distributed on the surface. While for the sample C, which covered with an ultra-thin heavy Cr-doped layer and 30 min vacuum atmosphere annealing, these nanorods almost disappeared. Due to the nanorods still could be seen on the surface of unannealed sample B, it is reasonable to deduce that the nanorods as well as ultra-thin covered layer has been completely integrated into the film matrix in sample C.
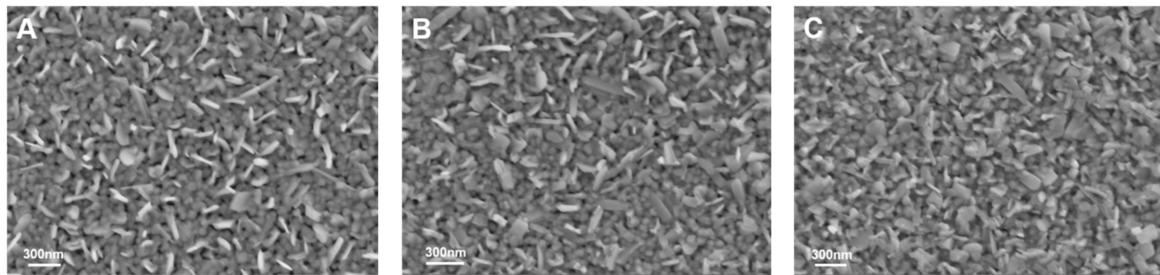
Figure 6. SEM images of as-grown pure VO$_2$ and an ultra-thin Cr-doped VO$_2$ layer. (**A**) is the pure VO$_2$ thin film, (**B**) is the unannealed Cr-doped VO$_2$ thin film, (**C**) is the Cr-doped VO$_2$ thin films annealing at 250 °C.

Temperature dependence of the electrical resistivity R curves of VO$_2$ films in heating process are shown in Figure 7. Abruptly change of resistance from low temperature to high temperature has been seen like IR-transmittance-temperature curve. We also noticed that the sheet resistance decreased in room temperature state after covered with heavy Cr-doped layer either unannealed or annealed.
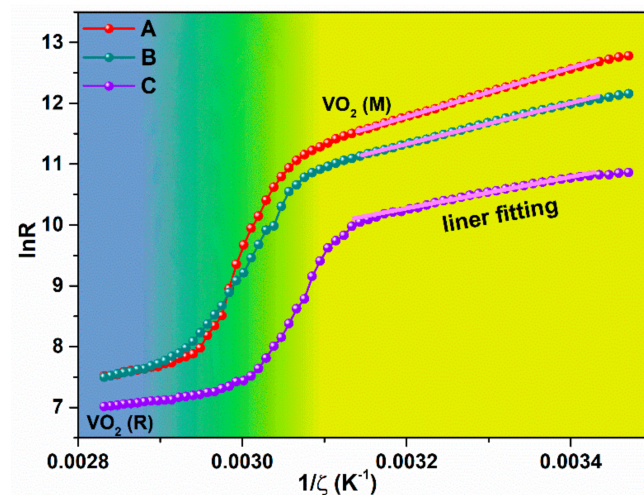

Figure 7. The *lnR–1/ζ* curve of all samples; the activation energy in the semiconductor phase is determined by linearly fitting the curve in low temperature state. (A) is the pure VO$_2$ thin film, (B) is the unannealed Cr-doped VO$_2$ thin film, (C) is the Cr-doped VO$_2$ thin films annealing at 250 °C.

The temperature dependence of electrical resistivity of VO$_2$ thin films in the semiconducting state can be expressed as [34]:

$$R = R_0 \exp\left(\frac{E_c - E_f}{k\zeta}\right) \tag{3}$$

where E_c is the energy of the edge of the conduction band, E_f is the Fermi level, k is the Boltzmann constant, and R_0 is the resistance at $\zeta \to \infty$.

Temperature coefficient of resistance (TCR) defined as the slope of the natural logarithm of electrical resistivity R in semiconducting state with temperature [35]:

$$TCR = \frac{1}{R}\frac{dR}{d\zeta} \tag{4}$$

Combining Equations (3) and (4) yields [36]

$$\Delta E = -k\zeta^2 \times TCR \tag{5}$$

This relation links the activation energy $\Delta E = E_c - E_f$ to TCR [37]. The activation energy in semiconductor state and conductivity at room temperature in our work are calculated (see Table 1). In ambient temperature, the carrier concentration of the three samples are 3.0163×10^{17} cm^{-3}, -6.8935×10^{17} cm^{-3}, and -1.9045×10^{18} cm^{-3}, respectively. It is clear that the VO$_2$ samples with heavy Cr-doped ultra-thin layer have higher conductivity and carrier concentration compared with the as-grown sample A. Due to the low conductivity in pure VO$_2$ bottom layer, it reveals that higher concentration carriers may only locate within the upper layer locally.

Table 1. Activation energy in semiconductor state and conductivity at room temperature of all samples.

Sample	A	B	C
activation energy ΔE (eV)	0.33	0.27	0.23
conductivity σ (S/m^2)	12.95	24.10	86.70
carrier concentration n (cm^{-3})	3.0163×10^{17}	-6.8935×10^{17}	-1.9045×10^{18}

The transition temperature can be affected by lattice strain [38], crystal size [39], ions doping [40], etc. From XRD spectra and SEM images, it can be seen that the diffraction peak position and grain size are basically unchanged in this work. So the phase transition temperature variation attributed to lattice strain and grain size is negligible in our research. It is reported that the phase transition behavior of the VO$_2$ thin films also could be influenced by carrier concentration. C. W. Zou [41] reported that the MIT could be controlled by modifying carrier density. For the Mott phase transition, the critical electron density n_c can be expressed as below equation:

$$n_c = \left(\frac{m^* e^2}{4 \hbar^2 \varepsilon} \right)^3 \tag{6}$$

where ε is the dielectric constant ($\sim$100 for VO$_2$), $\hbar$ is the Planck constant, and m^* and e are the effective mass and charge of an electron, respectively [42] For MIT in VO$_2$, $n_c \approx 3 \times 10^{18}$ cm^{-3} [43]. For sample B and C with low activation energy, the samples' surface is heavy Cr-doped layer and has high carrier concentration. It is easier to generate more carriers to reach the phase transition critical value of n_c and first induce local phase transition. MIT process will lead to carrier concentration increasing further. The carriers will diffuse from upper layer to bottom according to Fick's first law:

$$J = -D \frac{dn}{dx} \tag{7}$$

where D is carrier diffusion coefficient, J is diffusion flux, and dn/dx is the carrier concentration gradient [44]. With temperature increasing, the diffusion coefficient D and carrier concentration gradient dn/dx in the vertical direction of the film surface increased too. It will lead to higher carrier diffusion flux and phase transition occurring from upper layer to bottom layer gradually. It is reasonable to deduce that the upper heavy Cr-doped ultra-thin VO$_2$ film play the role of phase transition induction layer initially, which could reduce the phase transition temperature ζ_c due to the carrier injection (Figure 8a).

Figure 8b shows the temperature-dependent carrier concentration of pure VO$_2$ thin films. In the low-temperature insulating monoclinic state, the free-carriers type is holes. With temperature increasing, carriers gradually changed to electrons, and a sharp increasing of electrons concentration was observed when temperature increase to $\sim$70 °C, and the film turns into the metal rutile state.
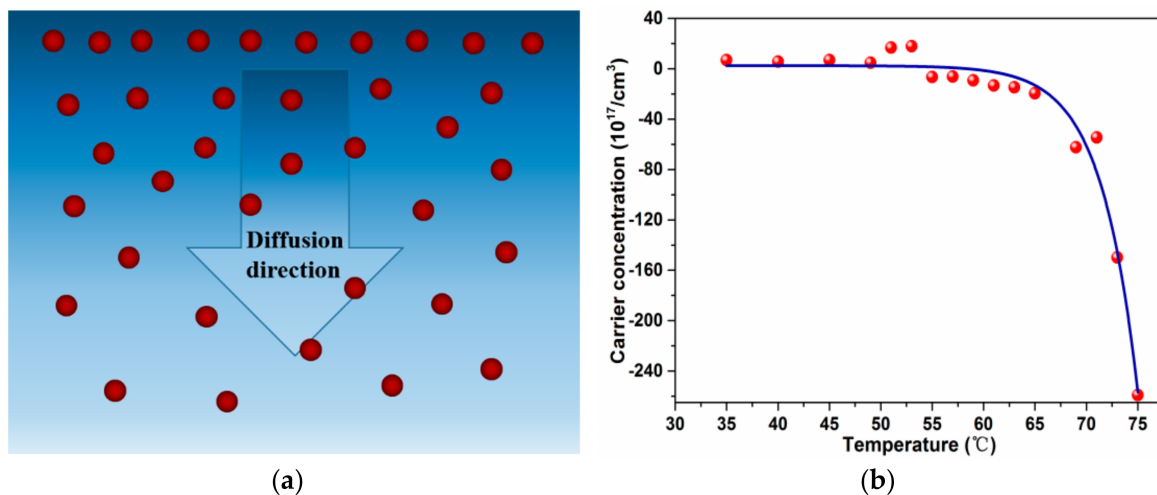
Figure 8. (**a**) Schematic of carrier distribution and diffusion in the cross-section of VO_2 thin films. (**b**) Temperature-dependent carrier concentration of pure VO_2 thin films.

4. Conclusions

In summary, VO_2 films were prepared by reactive pulsed magnetron sputtering, and a 3 nm ultra-thin heavy Cr-doped VO_2 layer prepared by reactive co-sputtering was employed to cover the pure VO_2 film. Then the covered samples were annealed in vacuum atmosphere. By characterizing the phase transition performances, microstructures, and electrical properties of the samples, phase transition temperature sharp decreasing of the covered ultra-thin heavy Cr-doped layer films was observed, and annealing could strengthen this effect. No obvious change of the microstructure and phase transition performance has been found before and after covering an ultra-thin layer on the pure VO_2 film. The three samples have almost the same solar energy modulation capability of $\Delta T_{IR,sol} = 12\%$. It is reasonable to deduce that the upper ultra-thin high Cr-doped layer, which has high carrier concentration, may act as induced-layer to generate more carriers to reach the threshold n_c and induced phase transition. This process will occur from upper layer to bottom layer gradually until phase transition occurs throughout the VO_2 film by carrier diffusion with temperature increasing. This is a simple method to reduce ζ_c and keep phase transition phase performance.

Author Contributions: Conceptualization, H.G. and D.Z.; methodology, H.G., Y.Y., Q.H., J.Q.; investigation, D.Z., Y.L., A.Z., P.F.; writing-original draft preparation, H.G., D.Z.; funding acquisition, D.Z. All authors have read and agreed to the published version of the manuscript.

Conflicts of Interest: The authors declare no conflict of interest.

References

1. Case, F.C. Modifications in the phase Transition Properties of Predeposited VO_2 Films. *J. Vac. Sci. Technol. A Vac. Surf. Film.* **1984**, *2*, 1509–1512. [CrossRef]
2. Boriskov, P.P.; Velichko, A.A.; Pergament, A.L.; Stefanovich, G.B.; Stefanovich, D.G. The Effect of Electric Field on Metal-Insulator Phase Transition in Vanadium Dioxide. *Tech. Phys. Lett.* **2002**, *28*, 406–408. [CrossRef]
3. Zhao, Y.; Hwan Lee, J.; Zhu, Y.; Nazari, M.; Chen, C.; Wang, H.; Bernussi, A.; Holtz, M.; Fan, Z. Structural, Electrical, and Terahertz Transmission Properties of VO_2 Thin Films Grown on c-, r-, and m-Plane Sapphire Substrates. *J. Appl. Phys.* **2012**, *111*, 053533. [CrossRef]
4. Hao, R.; Li, Y.; Liu, F.; Sun, Y.; Tang, J.; Chen, P.; Jiang, W.; Wu, Z.; Xu, T.; Fang, B. Electric Field Induced Metal–Insulator Transition in VO_2 Thin Film Based on FTO/VO_2/FTO Structure. *Infrared Phys. Technol.* **2016**, *75*, 82–86. [CrossRef]

5. Chen, S.; Ma, H.; Yi, X.; Xiong, T.; Wang, H.; Ke, C. Smart VO_2 Thin Film for Protection of Sensitive Infrared Detectors from Strong Laser Radiation. *Sens. Actuators A Phys.* **2004**, *115*, 28–31. [CrossRef]

6. Belyaev, M.A.; Putrolaynen, V.V.; Velichko, A.A.; Stefanovich, G.B.; Pergament, A.L. Field-Effect Modulation of Resistance in VO_2 Thin Film at Lower Temperature. *Jpn. J. Appl. Phys.* **2014**, *53*, 111102. [CrossRef]

7. Tselev, A.; Lavrik, N.V.; Kolmakov, A.; Kalinin, S.V. Scanning Near-Field Microwave Microscopy of VO_2 and Chemical Vapor Deposition Graphene. *Adv. Funct. Mater.* **2013**, *23*, 2635–2645. [CrossRef]

8. Arcangeletti, E.; Baldassarre, L.; Di Castro, D.; Lupi, S.; Malavasi, L.; Marini, C.; Perucchi, A.; Postorino, P. Evidence of a Pressure-Induced Metallization Process in Monoclinic VO_2. *Phys. Rev. Lett.* **2007**, *98*, 196406. [CrossRef]

9. Li, W.; Chang, S.; Wang, X.; Lin, L.; Bai, J. A Thermally Tunable Terahertz Bandpass Filter with Insulator-Metal Phase Transition of VO_2 Thin Film. *Optoelectron. Lett.* **2014**, *10*, 180–183. [CrossRef]

10. Ha, S.D.; Zhou, Y.; Fisher, C.J.; Ramanathan, S.; Treadway, J.P. Electrical Switching Dynamics and Broadband Microwave Characteristics of VO_2 Radio Frequency Devices. *J. Appl. Phys.* **2013**, *113*, 184501. [CrossRef]

11. Radu, I.P.; Martens, K.; Mertens, S.; Adelmann, C.; Shi, X.; Tielens, H.; Schaekers, M.; Pourtois, G.; Van Elshocht, S.; De Gendt, S.; et al. (Invited) Vanadium Oxide as a Memory Material. *ECS Trans.* **2011**, *35*, 233–243.

12. Huang, Z.; Chen, S.; Lv, C.; Huang, Y.; Lai, J. Infrared Characteristics of VO_2 Thin Films for Smart Window and Laser Protection Applications. *Appl. Phys. Lett.* **2012**, *101*, 191905. [CrossRef]

13. Liao, F.; Zhu, Z.; Yan, Z.; Yao, G.; Huang, Z.; Gao, M.; Pan, T.; Zhang, Y.; Li, Q.; Feng, X.; et al. Ultrafast Response Flexible Breath Sensor Based on Vanadium Dioxide. *J. Breath Res.* **2017**, *11*, 036002. [CrossRef] [PubMed]

14. Belyaev, M.A.; Velichko, A.A.; Boriskov, P.P.; Kuldin, N.A.; Putrolaynen, V.V.; Stefanovitch, G.B. The Field Effect and Mott Transistor Based on Vanadium Dioxide. *J. Sel. Top. Nano Electron. Comput.* **2014**, *1*, 26–30. [CrossRef]

15. Xiao, L.; Ma, H.; Liu, J.; Zhao, W.; Jia, Y.; Zhao, Q.; Liu, K.; Wu, Y.; Wei, Y.; Fan, S.; et al. Fast Adaptive Thermal Camouflage Based on Flexible VO_2/Graphene/CNT Thin Films. *Nano Lett.* **2015**, *15*, 8365–8370. [CrossRef]

16. Li, S.-Y.; Niklasson, G.A.; Granqvist, C.G. Thermochromic Fenestration with VO_2-Based Materials: Three Challenges and How They can be Met. *Thin Solid Film.* **2012**, *520*, 3823–3828. [CrossRef]

17. Li, S.; Li, Y.; Jiang, M.; Ji, S.; Luo, H.; Gao, Y.; Jin, P. Preparation and Characterization of Self-Supporting Thermochromic Films Composed of VO_2(M)@SiO_2 Nanofibers. *ACS Appl. Mater. Interfaces* **2013**, *5*, 6453–6457. [CrossRef]

18. Yuan, N.; Li, J.; Li, G.; Chen, X. The Large Modification of Phase Transition Characteristics of VO_2 Films on SiO_2/Si Substrates. *Thin Solid Film.* **2006**, *515*, 1275–1279. [CrossRef]

19. Chen, C.; Zhao, Y.; Pan, X.; Kuryatkov, V.; Bernussi, A.; Holtz, M.; Fan, Z. Influence of Defects on Structural and Electrical Properties of VO_2 Thin Films. *J. Appl. Phys.* **2011**, *110*, 023707. [CrossRef]

20. Appavoo, K.; Lei, D.Y.; Sonnefraud, Y.; Wang, B.; Pantelides, S.T.; Maier, S.A.; Haglund, R.F. Role of Defects in the Phase Transition of VO_2 Nanoparticles Probed by Plasmon Resonance Spectroscopy. *Nano Lett.* **2012**, *12*, 780–786. [CrossRef]

21. Piccirillo, C.; Binions, R.; Parkin, I.P. Nb-Doped VO_2 Thin Films Prepared by Aerosol-Assisted Chemical Vapour Deposition. *Eur. J. Inorg. Chem.* **2007**, *2007*, 4050–4055. [CrossRef]

22. Khan, G.R.; Asokan, K.; Ahmad, B. Room Temperature Tunability of Mo-doped VO_2 Nanofilms across Semiconductor to Metal Phase Transition. *Thin Solid Film.* **2017**, *625*, 155–162. [CrossRef]

23. Piccirillo, C.; Binions, R.; Parkin, I.P. Synthesis and Characterisation of W-doped VO_2 by Aerosol Assisted Chemical Vapour Deposition. *Thin Solid Film.* **2008**, *516*, 1992–1997. [CrossRef]

24. Wang, N.; Duchamp, M.; Dunin-Borkowski, R.E.; Liu, S.; Zeng, X.; Cao, X.; Long, Y. Terbium-Doped VO_2 Thin Films: Reduced Phase Transition Temperature and Largely Enhanced Luminous Transmittance. *Langmuir* **2016**, *32*, 759–764. [CrossRef]

25. Chae, B.G.; Kim, H.T.; Yun, S.J. Characteristics of W- and Ti-Doped VO_2 hin Films Prepared by Sol-Gel Method. *Electrochem. Solid State Lett.* **2008**, *11*, D53. [CrossRef]

26. Panagopoulou, M.; Gagaoudakis, E.; Boukos, N.; Aperathitis, E.; Kiriakidis, G.; Tsoukalas, D.; Raptis, Y.S. Thermochromic Performance of Mg-doped VO_2 Thin Films on Functional Substrates for Glazing Applications. *Sol. Energy Mater. Sol. Cells* **2016**, *157*, 1004–1010. [CrossRef]

27. Jin, P.; Tazawa, M.; Yoshimura, K.; Igarashi, K.; Tanemura, S.; Macák, K.; Helmersson, U. Epitaxial Growth of W-Doped VO_2/V_2O_3 Multilayer on α-Al_2O_3(110) by Reactive Magnetron Sputtering. *Thin Solid Film.* **2000**, *375*, 128–131. [CrossRef]

28. Batista, C.; Ribeiro, R.M.; Teixeira, V. Synthesis and Characterization of VO2-Based Thermochromic Thin Films for Energy-Efficient Windows. *Nanoscale Res. Lett.* **2011**, *6*, 301. [CrossRef]

29. Balin, I.; Wang, S.; Wang, P.; Long, Y.; Abdulhalim, I. Enhanced Transition-Temperature Reduction in a Half-Sphere Au/VO_2 Core-Shell Structure: Local Plasmonics Versus Induced Stress and Percolation Effects. *Phys. Rev. Appl.* **2019**, *11*, 034064. [CrossRef]

30. Schilbe, P. Raman Scattering in VO_2. *Phys. B Condens. Matter* **2002**, *316–317*, 600–602. [CrossRef]

31. Pan, M.; Liu, J.; Zhong, H.; Wang, S.; Li, Z.; Chen, X.; Lu, W. Raman Study of the Phase Transition in VO_2 Thin Films. *J. Cryst. Growth* **2004**, *268*, 178–183. [CrossRef]

32. Zhang, C.; Yang, Q.; Koughia, C.; Ye, F.; Sanayei, M.; Wen, S.-J.; Kasap, S. Characterization of Vanadium Oxide Thin Films with Different Stoichiometry Using Raman Spectroscopy. *Thin Solid Film.* **2016**, *620*, 64–69. [CrossRef]

33. Shibuya, K.; Tsutsumi, J.; Hasegawa, T.; Sawa, A. Fabrication and Raman Scattering Study of Epitaxial VO_2 Films on MgF_2 (001) Substrates. *Appl. Phys. Lett.* **2013**, *103*, 021604. [CrossRef]

34. Wang, Y.; Zhang, Z.; Zhu, Y.; Li, Z.; Vajtai, R.; Ci, L.; Ajayan, P.M. Nanostructured VO_2 Photocatalysts for Hydrogen Production. *ACS Nano* **2008**, *2*, 1492–1496. [CrossRef]

35. Pan, M.; Zhong, H.; Wang, S.; Liu, J.; Li, Z.; Chen, X.; Lu, W. Properties of VO_2 Thin Film Prepared with Precursor VO_2. *J. Cryst. Growth* **2004**, *265*, 121–126. [CrossRef]

36. Liu, H.; Wan, D.; Ishaq, A.; Chen, L.; Guo, B.; Shi, S.; Luo, H.; Gao, Y. Sputtering Deposition of Sandwich-Structured V_2O_5/Metal(V,W)/V_2O_5 Multilayers for the Preparation of High-Performance Thermally Sensitive VO_2 Thin Films with Selectivity of VO_2(B) and VO_2(M) Polymorph. *ACS Appl. Mater. Interfaces* **2016**, *8*, 7884–7890. [CrossRef]

37. Mai, L.Q.; Hu, B.; Hu, T.; Chen, W.; Gu, E.D. Electrical Property of Mo-Doped VO_2 Nanowire Array Film by Melting−Quenching Sol−Gel Method. *J. Phys. Chem. B* **2006**, *110*, 19083–19086. [CrossRef]

38. Lee, D.; Lee, J.; Song, K.; Xue, F.; Choi, S.-Y.; Ma, Y.; Podkaminer, J.; Liu, D.; Liu, S.-C.; Chung, B.; et al. Sharpened VO_2 Phase Transition via Controlled Release of Epitaxial Strain. *Nano Lett.* **2017**, *17*, 5614–5619. [CrossRef]

39. Dai, L.; Cao, C.; Gao, Y.; Luo, H. Synthesis and Phase Transition Behavior of Undoped VO_2 with a Strong Nano-Size Effect. *Sol. Energy Mater. Sol. Cells* **2011**, *95*, 712–715. [CrossRef]

40. Ji, H.; Wei, J.; Natelson, D. Modulation of the Electrical Properties of VO_2 Nanobeams Using an Ionic Liquid as a Gating Medium. *Nano Lett.* **2012**, *12*, 2988–2992. [CrossRef]

41. Chen, F.H.; Fan, L.L.; Chen, S.; Liao, G.M.; Chen, Y.L.; Wu, P.; Song, L.; Zou, C.W.; Wu, Z.Y. Control of the Metal–Insulator Transition in VO_2 Epitaxial Film by Modifying Carrier Density. *ACS Appl. Mater. Interfaces* **2015**, *7*, 6875–6881. [CrossRef] [PubMed]

42. Stefanovich, G.; Pergament, A.; Stefanovich, D. Electrical Switching and Mott Transition in VO_2. *J. Phys. Condens. Matter* **2000**, *12*, 8837–8845. [CrossRef]

43. Pergament, A. Metal–Insulator Transition: The Mott Criterion and Coherence Length. *J. Phys. Condens. Matter* **2003**, *15*, 3217–3223. [CrossRef]

44. Kasırga, T.S.; Coy, J.M.; Park, J.H.; Cobden, D.H. Visualization of One-Dimensional Diffusion and Spontaneous Segregation of Hydrogen in Single Crystals of VO_2. *Nanotechnology* **2016**, *27*, 345708. [CrossRef] [PubMed]